Desalination and Water Treatment
www.deswater.com
doi: 10.5004/dwt.2020.26046

196 (2020) 247–255
August

A facile vapor deposition synthesis of g-C_3N_4/SiO_2 nanocomposite with large specific surface area and enhanced photocatalytic activity

Fang-yan Chen*, Min-keng He, Yu-bin Tang, Cheng-yi He, Ke-ke Shu, Ming-yang Li

School of Environmental and Chemical Engineering, Jiangsu University of Science and Technology, Zhenjiang Jiangsu, 212003 China, Tel. +86-511-85605157; email: chenfangyan@just.edu.cn (F.-y. Chen), Tel. +86-511-85605156; email: 1026709345@qq.com (M.-k. He), Tel. +86-511-84448601; email: ybbill@163.com (Y.-b. Tang), Tel. +86-511-85605156; email: 742256533@qq.com (C.-y. He), Tel. +86-511-85605156; email: 1149939830@qq.com (K.-k. Shu), Tel. +86-511-85605156; email: 2727838178@qq.com (M.-y. Li)

Received 2 October 2019; Accepted 29 April 2020

ABSTRACT

A core-shell g-C_3N_4/SiO_2 nanocomposite was successfully synthesized by depositing g-C_3N_4, obtained from the sublimation of melamine and subsequent polymerization reaction in the gaseous phase, on the nano-silica. The as-prepared g-C_3N_4/SiO_2 was characterized by X-ray diffraction, Fourier transform infrared spectroscopy, transmission electron microscopy, X-ray photoelectron spectroscopy, N_2 adsorption–desorption, UV-vis diffuse reflectance spectroscopy. The visible-driven photocatalytic activity of g-C_3N_4/ SiO_2 was evaluated by the degradation of tetracycline. The results indicate that the specific surface area of g-C_3N_4/SiO_2 is 97.32 m^2/g, which is 6.74 times as high as that of bulk g-C_3N_4 (14.44 m^2/g). Compared to bulk g-C_3N_4, g-C_3N_4/SiO_2 composite exhibits significantly enhanced photocatalytic activity for degradation of tetracycline and can degrade 72.7% of tetracycline within 60 min under visible-light irradiation. The photodegradation rate constant of tetracycline over g-C_3N_4/SiO_2 is 7.2 times as high as that over bulk g-C_3N_4. The greatly enhanced photocatalytic activity of g-C_3N_4/SiO_2 is due to coupling enlarged surface areas with the contribution of SiO_2 in inhibition of the recombination of photo-induced electron-hole pair.

Keywords: Photocatalyst; Graphitic carbon nitride; Silica; Composite; Tetracycline; Visible light

1. Introduction

In recent decades, visible-light-driven photocatalysts have been extensively investigated in energy and environment areas owing to their ability for solar energy conversion [1–7]. Of various kinds of present photocatalysts, graphitic carbon nitride (g-C_3N_4) has been considered as a desirable visible-light photocatalyst due to its medium bandgap of 2.7 eV, free of heavy metal, and highly chemical stability [8,9]. However, small specific surface areas and high recombination rate of charged carriers greatly restrict its photocatalytic activity. Thus, many kinds of methods and techniques, such as morphology control [10,11], element doping [12,13], and combining with other materials to construct composite catalysts [14,15], have been adopted to enhance the photocatalytic performance of g-C_3N_4. Morphology control is used to increase the activity sites of photocatalyst to further enhance photocatalytic activity. Nanostructure, one of morphology control, is mainly used to increase the activity sites through enhancing the specific surface area of photocatalyst, while, composite structure and element doping are mainly used to improve photocatalytic

* Corresponding author.

activity via regulation of bands gap and inhibition of recombination of photo-induced charges. Among these modification methods, construction of composite photocatalysts is dominant strategy. Large amount of composites based on g-C_3N_4 have been reported [16–19].

Silica has hardly any photocatalytic activity because of its inherent characteristics as an insulator. It is usually employed as a hard template in preparation of photocatalyst so as to enhance the specific surface area of photocatalysts [20–22]. For example, some researchers employed nanoscale SiO_2 as a hard template to fabricate mesoporous, multi-shell, and hollow nanoscale g-C_3N_4 [23–25]. During preparation of catalysts, SiO_2 is needed to be removed via hydrofluoric acid, which is time-consuming, high-cost, and harm to the environment. Nevertheless, some reports confirmed that the construction of the composite based on g-C_3N_4 and SiO_2 is beneficial for improving photocatalytic activity of g-C_3N_4 because the coexistence of silica both increase specific surface area of C_3N_4 and also promote separation of photo-induced electron-hole pairs [26]. Up to now, there are only few reports on composite of g-C_3N_4 and SiO_2. Lin et al. [27] have reported a core-shell g-C_3N_4/SiO_2 nanosphere synthesized by heating mixture of SiO_2 nanospheres and cyanamide in a nitrogen atmosphere. However, the specific surface area of the obtained g-C_3N_4/SiO_2 was only 8–13 m^2/g. Wang et al. [28] have synthesized the g-C_3N_4/SiO_2 composite by calcining a mixture of SiO_2 nanoparticles and melamine at 520°C. The prepared composites own a specific surface area of 19–52 m^2/g. Nevertheless, the role of SiO_2 in composite has not discussed. Hao et al. [26] have reported that they prepared g-C_3N_4/SiO_2 composites by heating precursor melamine and SiO_2 and investigated the critical role of SiO_2 in inhibiting the recombination of photo-generated carriers. But the g-C_3N_4 in the composite is still bulk g-C_3N_4 in micron size, and the largest specific surface area of the composites is only 36.8 m^2/g. As known to all, large surface area plays considerable roles in improving the activity of the photocatalysts. Therefore, it is still of important interest to increase the surface area of g-C_3N_4/SiO_2 composite to promote the photocatalytic activity.

Herein, we report that a g-C_3N_4/SiO_2 nanocomposite with large specific surface area and excellent photocatalytic activity is synthesized by a facile vapor deposition. The photocatalytic activity of as-prepared g-C_3N_4/SiO_2 was evaluated by degradation of tetracycline under visible-light irradiation. For comparison, the nano-g-C_3N_4 was prepared by etching silica from SiO_2/g-C_3N_4. The process of charge carries transfer on the interface of composite g-C_3N_4/SiO_2 was also discussed.

2. Experimental

2.1. Chemicals

Melamine, tetracycline hydrochloride, hydrofluoric acid, isopropyl alcohol, potassium iodide (KI) and L(+) ascorbic acid were purchased from Sinopharm Group Chemical Reagent Co., Ltd., China. All reagents were of analytical grade and used as received without further purification. Nano-silica with diameter of 15 nm was obtained from Shanghai Aladdin Biochemical Technology Co., Ltd., China.

2.2. Preparation of photocatalyst

2.2.1. Preparation of g-C_3N_4/SiO_2 composite

A cylindrical beaker was put upside down in a large crucible with a cover. 0.1 g of silica was loaded on the top of the beaker, and the melamine was placed on the bottom of the crucible. The crucible is covered and put into a muffle furnace. Then the muffle furnace was heated to 520°C at a heating rate of 15°C/min and held for 240 min and naturally cooled to room temperature. During heating treatment, g-C_3N_4 was obtained by sublimation of melamine and subsequent polymerization, and deposited on the surface of nano-silica located on the top of the beaker to get g-C_3N_4/SiO_2 composite. Different amounts of melamine (20, 30, and 40 g) were used to increase g-C_3N_4 deposition, the resultant nanocomposites were marked as SiO_2/CN-20, SiO_2/CN-30, and SiO_2/CN-40, respectively.

2.2.2. Preparation of nano-g-C_3N_4

For comparison, the nano-g-C_3N_4 was also prepared by eliminating silica in nano-g-C_3N_4/SiO_2. SiO_2/CN-30 and a certain amount of hydrofluoric acid were placed in a centrifuge tube and centrifuged at 12,000 r/min. The supernatant was poured off, and the precipitants were washed with deionized water until the supernatant was neutral, dried at 60°C overnight to obtain nano-g-C_3N_4, denoted as nano-CN.

2.2.3. Preparation of bulk g-C_3N_4

Twenty grams of melamine was heated in a muffle furnace at 520°C with heating rate of 15°C/min for 240 min, naturally cooled down, and the yellow products in the crucible were ground to obtain bulk g-C_3N_4, marked as CN.

2.3. Characterization of the photocatalysts

X-ray diffraction (XRD) patterns of samples were obtained from D8-Advance X-ray diffractometer (Bruker AXS C, Germany) with a Cu-Ka radiation (λ = 1.5406 Å). The scanning electron microscopy (SEM) images were observed by S-4800 field emission SEM (Hitachi, Japan) and the transmission electron microscopy (TEM) images were obtained by JEM-2100 TEM (Japan Electronics, Japan). UV-vis diffuse reflectance spectra were collected on UV-2550 UV-vis spectrophotometer (Shimadzu, Japan). Elemental composition and chemical valence of the samples were characterized by ESCALAB-250i X-ray photoelectron spectroscope (Thermo Fisher Scientific, USA). The PL spectra of the photocatalysts were recorded on F4500 Fluorescence spectrometer (Hitachi, Japan). The specific surface area was determined by N_2 adsorption–desorption isotherm obtained from Autosorb-1-c sorption analyzer (Quantachrome, USA). Transient photocurrent measurements were conducted on CHI 660D electrochemical workstation (Chenhua Instrument, China).

2.4. Photocatalytic degradation of tetracycline

The photocatalytic activity of as-obtained samples was evaluated by photocatalytic degradation of tetracycline hydrochloride. Fifty milligrams of the photocatalysts were dispersed to 100 mL of tetracycline hydrochloride solution with initial concentration of 10 mg/L and stirred in the dark for 60 min to achieve adsorption–desorption equilibrium. Then, the solution was irradiated by a xenon lamp with a

420 nm cut-off filter and a focused intensity of 89 mV/cm^2. The distance from the solution to the xenon lamp is 12 cm. At 10 min intervals, 3 mL suspension were taken out and centrifuged, and then the concentration of tetracycline hydrochloride in the supernatant was determined according to absorbance at 357 nm by a UV-Vis spectrophotometer.

3. Results and discussion

3.1. X-ray diffraction

Fig. 1 is the XRD patterns of bulk g-C_3N_4, nano-g-C_3N_4, and g-C_3N_4/SiO_2 composite. As given in Fig. 1, the characteristic diffraction peaks of the (100) and (002) crystal plane of g-C_3N_4 are found in all the XRD patterns, which are attributed to the repeating of in-plane N-bridged tri-s-triazine units and the interlayer stacking of conjugated aromatic segments, respectively [27,29]. However, the (100) diffraction peak of SiO_2/CN-*X* (*X* = 20, 30, and 40) and nano-CN down-shift from 12.8° for bulk g-C_3N_4 to 12.7°. It is suggested, compared to bulk g-C_3N_4, that the in-plane hole to hole distance of g-C_3N_4 phase in SiO_2/CN-*X* and nano-CN increase, which can lead to increase in the specific surface area. Furthermore, the (002) diffraction angle of SiO_2/CN-*X* (*X* = 20, 30, and 40) and nano-CN right-shift from 27.4° of 2θ for g-C_3N_4 to 27.6°of 2θ (shown in insertion of Fig. 1), meaning decrease of the interlayer distance of g-C_3N_4 in SiO_2/CN-*X* and nano-CN compared to bulk g-C_3N_4. The difference in crystal phase between the SiO_2/CN-*X*, nano-CN and the bulk g-C_3N_4 is due to nanosizing of g-C_3N_4 in SiO_2/CN-*X* and nano-CN [29].

3.2. FT-IR spectra

The Fourier transform infrared (FT-IR) spectra of nano-CN, SiO_2, and SiO_2/CN-30 are given in Fig. 2. In the infrared spectrum of SiO_2, the sharp absorption peak at 478; 1,114; and 788 cm^{-1} are attributed to Si–O–Si bending vibration, Si–O–Si asymmetric stretching vibration and Si–OH bending vibration. While the broad band around 3,500 cm^{-1} is ascribed to the O–H stretching vibration of H_2O adsorbed on the surface of silica [27,30]. However, a few of new absorption bands are found in the infrared spectrum of SiO_2/CN-30. Among these new absorption bands, the sharp peak at 808 cm^{-1} belongs to the out-of-plane bending vibration of triazine ring of g-C_3N_4. The intense absorption band between 1,100 and 1,670 cm^{-1} is assigned to the characteristic stretching mode of heterocycles in g-C_3N_4. Of them, the peak at 1,240 and 1,340 cm^{-1} correspond to the stretching vibration of C–N group, and the sharp absorption peak at 1,408 and 1,571 cm^{-1} belong to characteristic C=N stretching vibration. The broad band located at 3,000–3,300 cm^{-1} is perhaps due to the terminal N–H stretching vibration of g-C_3N_4 [29]. The above mentioned results indicate that SiO_2/CN is a composite of g-C_3N_4 and silica. In the spectrum of nano-CN, only the characteristic peak of g-C_3N_4 at 808; 1,100–1,670; and 3,000–3,300 cm^{-1} are observed, no peaks related to silica are found, It is suggested that the silica, as a template, has been eliminated thoroughly via HF etching process and nano-CN is the nanosized g-C_3N_4 free of silica.

3.3. SEM and TEM

Fig. 3 exhibits the SEM and TEM images of SiO_2/CN-30, nano-CN and bulk g-C_3N_4. As shown in Figs. 3a and b, g-C_3N_4/SiO_2 composite exist as agglomerated small particles with diameter of about 100 nm, while bulk g-C_3N_4 is bulky particle with a size of approximate micron level. TEM images of SiO_2/CN-30 (Fig. 3c) shows that SiO_2 nanoparticles are covered by a thin layer of incompact g-C_3N_4 to form core-shell structured composite. Figs. 3d and e indicate that nano-CN is hollow nanoparticle, confirming that template SiO_2 has been removed in preparation of nano-CN.

3.4. Specific surface areas

Fig. 4 gives the N_2 adsorption–desorption isotherm and pore size distribution curve of the samples. As can be seen from Fig. 4, the type of adsorption–desorption isotherm

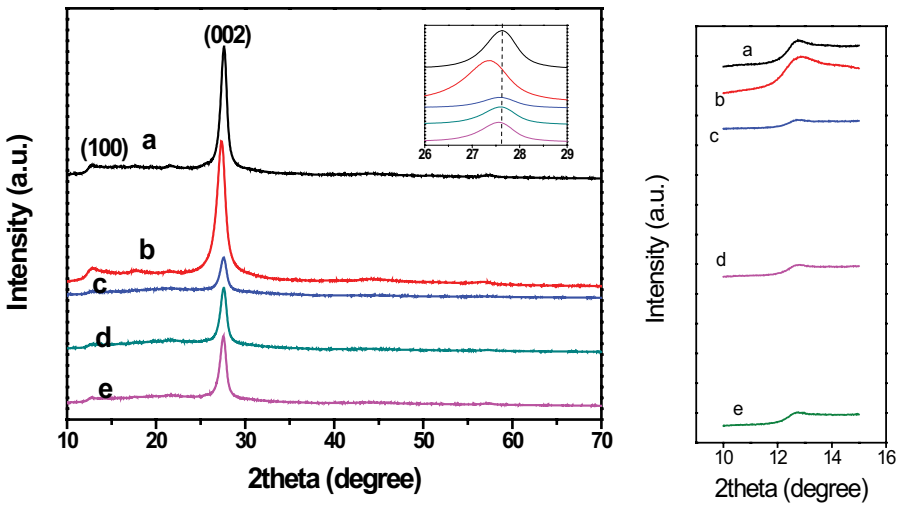

Fig. 1. XRD patterns of (a) nano-CN, (b) CN, (c) SiO_2/CN-20, (d) SiO_2/CN-30, and (e) SiO_2/CN-40.

of SiO_2/CN-30 and nano-CN suggests that SiO_2/CN-30 and nano-CN is characteristic of mesoporous structure. Meanwhile, the curve of pore size distribution (inserted in Fig. 4) indicates that most of the pores diameter in SiO_2/CN-30 and nano-CN are in the range of 2–50 nm. According to Brunauer–Emmett–Teller model, the specific surface areas of SiO_2/CN-30, nano-CN and CN are calculated to be 97.32, 99.37, and 14.44 m^2/g, respectively. It is

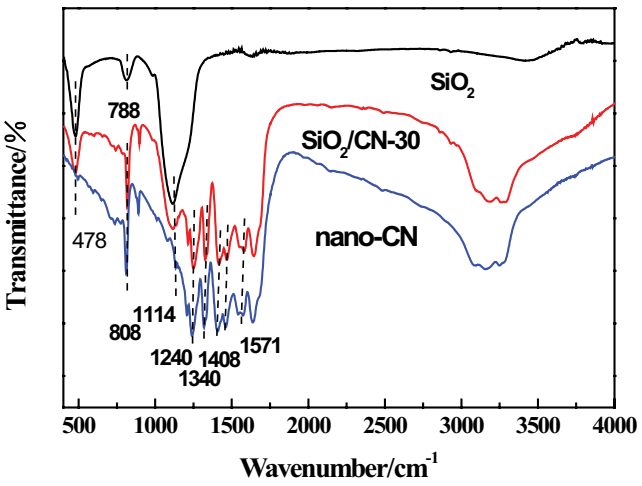

Fig. 2. FT-IR spectra of SiO_2, SiO_2/CN, and nano-CN.

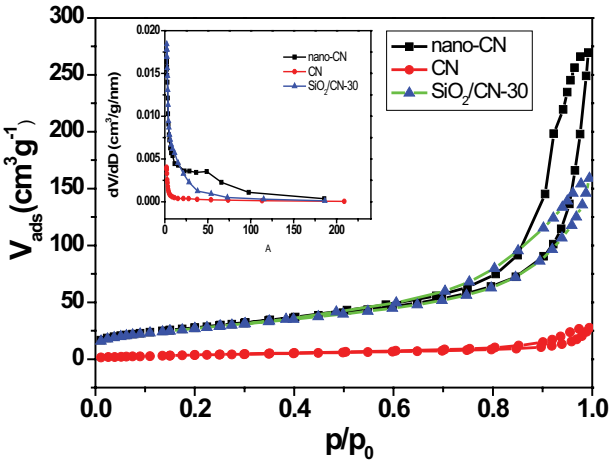

Fig. 4. Nitrogen adsorption–desorption isotherm and pore size distribution curve of nano-CN, CN, and SiO_2/CN-30.

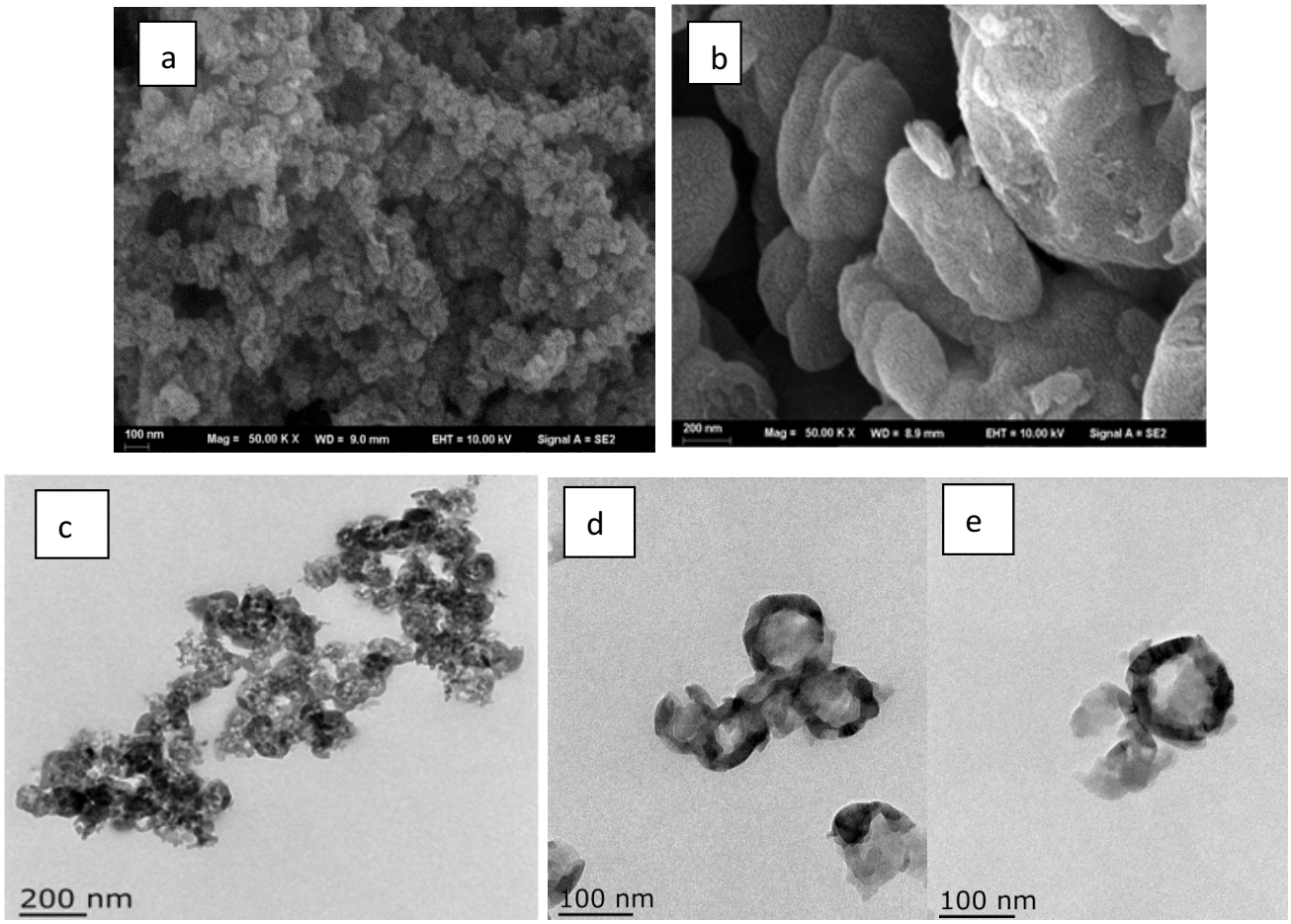

Fig. 3. SEM images of (a) SiO_2/CN-30 and (b) CN, TEM images of (c) SiO_2/CN-30 and (d and e) nano-CN.

noted that specific surface areas of SiO_2/CN-30 is 6.74 times as high as that of CN and is even close to the surface areas of hollow nano-CN. The results of specific surface areas confirm that vapor deposition method is favor of constructing g-C_3N_4/SiO_2 nanocomposite with large specific surface area.

3.5. X-photoelectron spectra

Fig. 5 shows the XPS spectra of SiO_2/CN-30 composite. As depicted in Fig. 5, N 1s, C1s, O1s, and Si 2p peaks are observed in the survey spectrum (Fig. 5a), suggesting that SiO_2/CN-30 is primarily consist of C, N, Si, and O element. In the high resolution spectrum of N 1 s (Fig. 5b), N 1s spectrum can be deconvoluted into three peaks with the binding energy of 398.7, 400.3, and 401.4 eV, corresponding to C–N=C, N–$(C)_3$, and C–N–H, respectively [29]. In the high-resolution spectrum of C 1s (Fig. 5c), the binding energy of 288.01 eV is attributed to sp2 hybridized carbon atom from the tri-s-triazine ring of g-C_3N_4 [25]. In the high resolution spectrum of Si 2p (Fig. 5d), the peak at

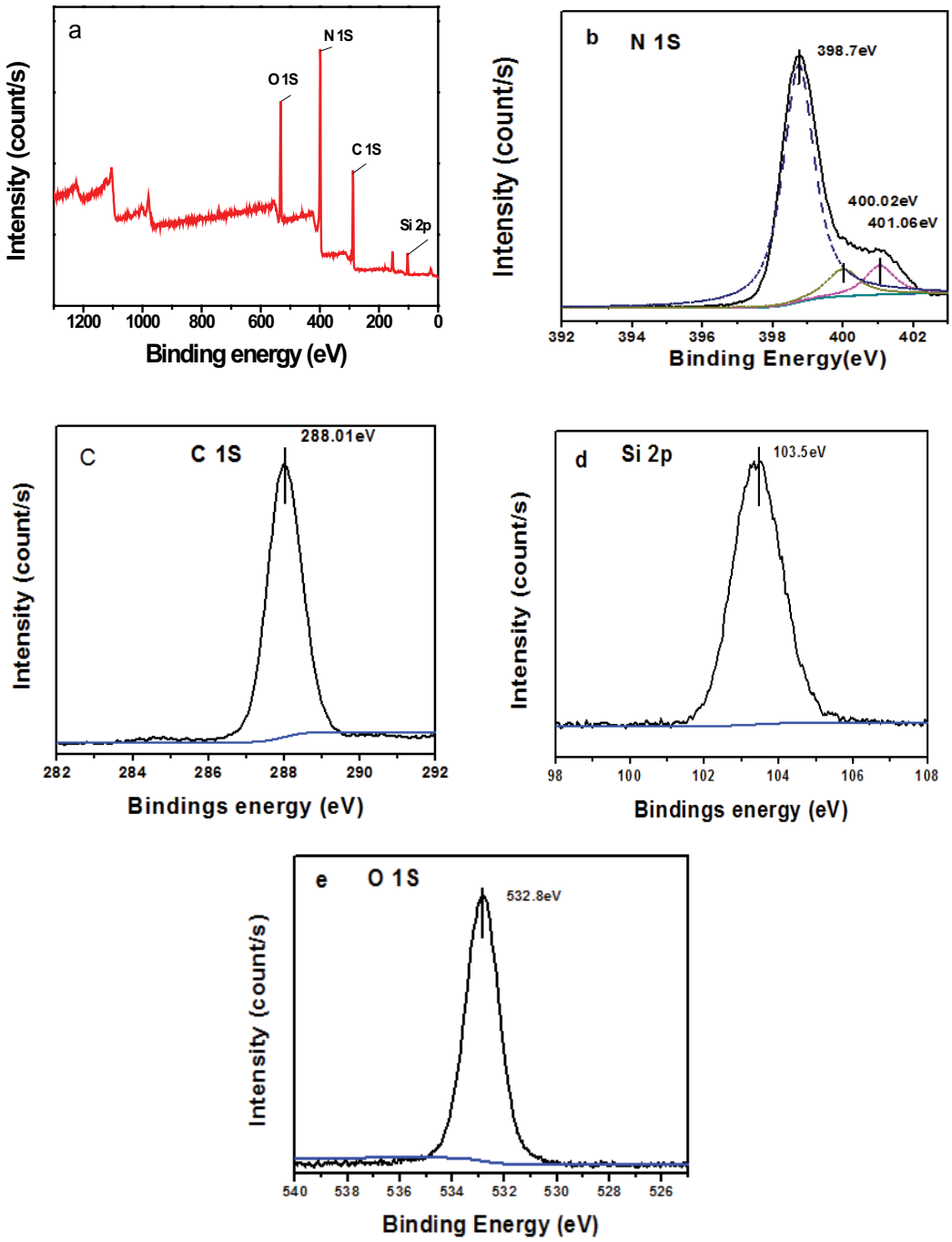

Fig. 5. XPS survey spectrum of SiO_2/CN-30 (a) and high-resolution spectra of N 1s (b), C1s (c), Si 2p (d), and O 1s (e).

the binding energy of 103.5 eV is designated to Si^{4+} of the nano-silica, and the binding energy of 532.8 eV shown in Fig. 5e corresponds to the oxygen in Si–O–Si from nano-silica [22]. The XPS results further confirmed that the g-C_3N_4/SiO_2 composite has been successfully synthesized by vapor deposition method.

3.6. UV-vis diffuse reflectance spectroscopy

Fig. 6a shows the UV-vis diffuse reflectance spectra of CN, SiO_2/CN-30 and nano-CN. As seen in Fig. 6a, compared with CN, the absorption band edge of SiO_2/CN-30 and nano-CN shows a slight blue-shift but is still within the range of visible light. The band gap of a semiconductor can be obtained by the Tauc formula $\alpha h\nu = A(h\nu - E_g)^{n/2}$, where α, h, ν, A, and E_g are the absorption coefficient, the Planck constant, the optical frequency, a constant, and the band gap, respectively. For the direct bandgap semiconductor g-C_3N_4, the value of n is 1 [25]. The plots of $(\alpha h\nu)^2$ vs. $(h\nu)$ for CN, SiO_2/CN-30, and nano-CN are presented in Fig. 6b. According to the intercept of the tangent of the curve $(\alpha h\nu)^2$ – $(h\nu)$ on X-axis, the band gap of CN, SiO_2/CN-30, and nano-CN are obtained to be 2.55, 2.57, and 2.75 ev, respectively. The increase in the band gap energy of SiO_2/CN-30 composite and nano-CN is attributed to the formation of nano-sized g-C_3N_4 which produces a quantum size effect [28].

The valence band-edge potential (E_{VB}) of a semiconductor can be calculated by the empirical equation $E_{VB} = X - E_e + 0.5E_g$ [26], where E_e is the free electrons energy on the hydrogen scale (about 4.5 eV), X is the electronegativity of the semiconductor (The X valence for g-C_3N_4 is 4.72), E_g is the band gap of the semiconductor. Given the equation above, E_{VB} of as-prepared g-C_3N_4 is calculated to be 1.50 eV. According to the equation $E_{CB} = E_{VB} - E_g$, the conduction band-edge potential (E_{CB}) of g-C_3N_4 is obtained to be –1.05 eV.

3.7. Photoluminescence spectra

Fig. 7 gives the PL spectra of CN and SiO_2/CN-30 at 385 nm excitation. As shown in Fig. 7, the PL intensity of SiO_2/CN-30 is obviously lower than that of CN, revealing that the existence of SiO_2 in SiO_2/CN-30 composite can hinder the recombination of photo-induced electron-hole pairs. The positive influence of SiO_2 on inhibiting the recombination of charged carries is perhaps attributed to defects and vacancy sites on the surface of SiO_2 [27,28]. Therefore, it can be speculated, based on PL spectra, that SiO_2/CN-30 would show higher photocatalytic activity than CN.

3.8. Photocurrent response

It is well-known that photocurrent response of semiconductor catalysts under irradiation of UV-Vis light is a crucial evidence for confirming the separation and migration of photo-generated electron-holes. To further investigate the effect of SiO_2 on hindering the recombination of charged carries, transient photocurrent responses test of SiO_2/CN-30 under visible light was carried out and the result is shown in Fig. 8. As a comparison, the transient photocurrent responses of nano-CN and CN are also given in Fig. 8. As can be seen from Fig. 8, SiO_2/CN-30 exhibit significantly higher photocurrent density than nano-CN and CN, suggesting that combination of SiO_2 and g-C_3N_4 greatly promotes the migration of electrons and thus inhibit the

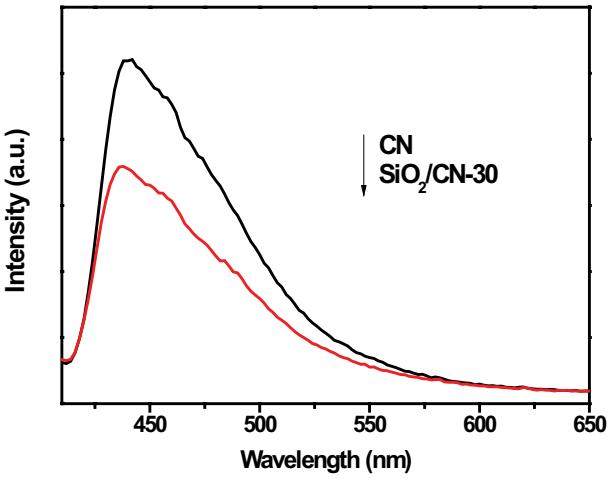

Fig. 7. Photoluminescence spectra of CN and SiO_2/CN-30.

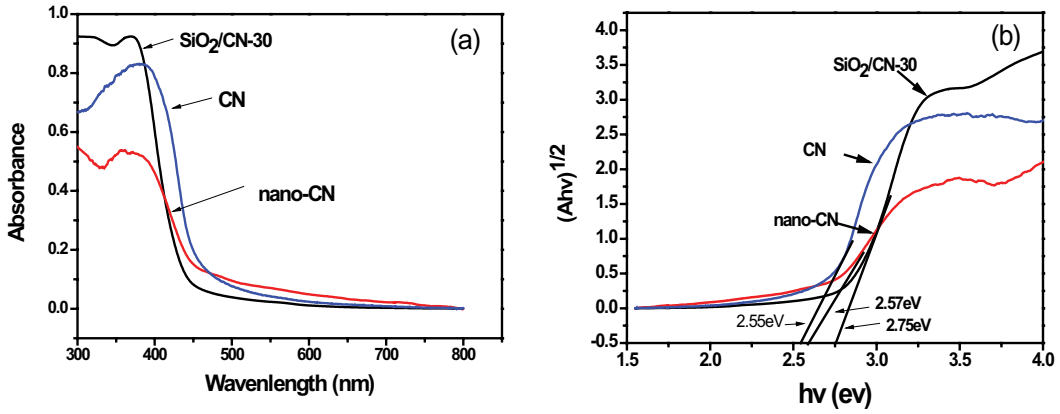

Fig. 6. UV-vis absorption spectra of (a) CN, (b) SiO_2/CN-30, and (c) nano-CN.

recombination of photo-induced electron-hole pairs. It may be due to that fact that the existence of defects and impurity levels of SiO_2 result in electrons migration to SiO_2 surface and consequent inhibition of recombination of photo-induced electron-hole pairs [22]. The higher photocurrent density of naco-CN than CN is probably attributed to the nanostructure of naco-CN and correspondingly enlarged surface areas. The results from photocurrent response further demonstrate that SiO_2 in SiO_2/CN composite play significantly important role in promoting the separation of charge carries and resultantly enhancing photocatalytic activity. In addition, only a slight decrease in photocurrent density of SiO_2/CN after five on-off cycles of intermittent visible light irradiation implies the stability of SiO_2/CN.

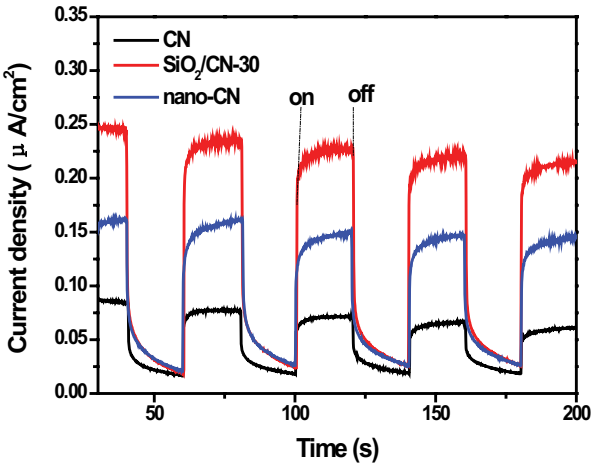

Fig. 8. Transient photocurrent response of CN, SiO_2/CN-30, and nano-CN under visible light ($\lambda > 420$ nm).

3.9. Photocatalytic performance

The photodegradation of antibiotics tetracycline under visible-light irradiation was conducted to evaluate visible-light-driven activity of SiO_2/CN, and the results are presented in Fig. 9a. As can be seen in Fig. 10, individual silica shows hardly any photocatalytic activity for degradation of tetracycline. The bulk g-C_3N_4 exhibits inferior activity with a degradation rate of tetracycline of 17.3% within 60 min. The degradation rate of tetracycline in the presence of nano-CN is 60.3%. However, SiO_2/CN-X (X = 20, 30, and 40) composite exhibits observably higher activity than nano-CN and CN. Of these composites, SiO_2/CN-30 shows the highest activity with a degradation of tetracycline of 72.7%.

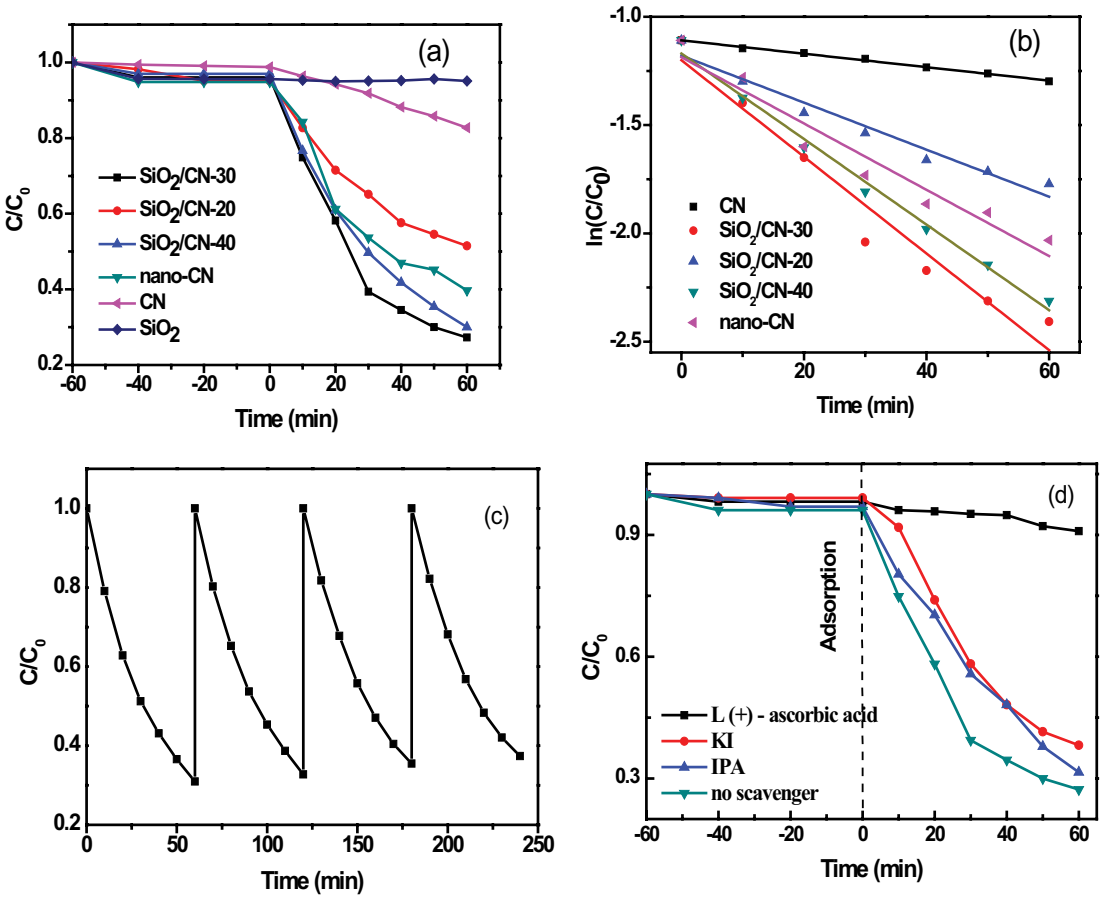

Fig. 9. (a) Photocatalytic degradation of tetracycline under visible light, (b) kinetic curve of photocatalytic degradation of tetracycline, (c) photocatalytic degradation of tetracycline in cycling test of SiO_2/CN-30, and (d) photocatalytic activity of SiO_2/CN-30 for degradation in the presence of different radical scavenger.

The rate constant of tetracycline degradation over CN, nano-CN, SiO_2/CN-*X* (*X* = 20, 30, and 40), obtained by the gradient of corresponding ln (C_t/C_0) vs. *t* curve shown in Fig. 9b, are 0.0031, 0.0153, 0.0109, 0.0223, and 0.0198 1/min, respectively. The rate constant of tetracycline degradation over SiO_2/CN-30 is 7.2 and 1.5 times as high as that over CN and nano-CN, respectively. Compared to CN, the enhanced photocatalytic activity of nano-CN is attributed to the fact that the obviously enlarged specific surface area of nano-CN can supply much more active sites for photo-generated charge carries to take part in catalytic reaction and thus suppress the recombination of photo-produced electron and hole. It is noted that the photocatalytic activity of SiO_2/CN composites is greatly higher than that of nano-CN free of SiO_2 though both of them own similar surface areas. It is suggested that, besides for specific surface areas, the existence of SiO_2 can also contribute to the greatly enhanced photocatalytic activity of SiO_2/CN. As a result, the enhanced photocatalytic activity of g-C_3N_4/SiO_2 composite is attributed to coupling effect between enlarged surface areas and contribution of SiO_2 in inhibition of the recombination of photo-induced electron-hole pairs.

Considering that the stability of photocatalyst is an important aspect of photocatalytic activity, the cycling degradation tests was carried out to evaluate the stability of SiO_2/CN-30 and the results are given in Fig. 9c. It can be seen from Fig. 9c, the photocatalytic efficiency of tetracycline only decreased slightly after being used four cycles, suggesting that SiO_2/CN-30 own excellent stability and reusability.

In order to investigate the contribution of active species during degradation of tetracycline, radical trapping tests are conducted. L(+)-ascorbic acid, potassium iodide (KI), and isopropanol (IPA) were selected to eliminate superoxide radical ($^{\bullet}O^{2-}$), hole (h^+) and hydroxyl radical ($^{\bullet}OH$), respectively. The degradation of tetracycline in the presence of scavengers is shown in Fig. 9d. It ca be seen from Fig. 9d, the photodegradation rate of tetracycline decreased from 72.7% to 9.2% after addition of L(+)-ascorbic acid, indicating that the $^{\bullet}O^{2-}$ plays the most important role. However, the photodegradation rate of tetracycline in the presence of KI and IPA are 61.8% and 68.5%, suggesting that addition of KI and IPA slightly inhibit degradation of tetracycline. Thus, hole and hydroxyl radical participate in degradation of tetracycline to some extent.

Given the results above, the schematics for photocatalytic degradation of tetracycline with SiO2/CN-30 composite is proposed and depicted in Fig. 10. It should be noted that SiO_2, as an insulator, is difficult to be triggered by visible-light to produce photo-induced electrons and holes. However, the previous literature has reported that nanoscale SiO_2 has some impurity energy levels due to the presence of defects [26]. Herein, the impurity energy levels of SiO_2 are given in Fig. 10. As shown in Fig. 10. The g-C_3N_4 in SiO_2/CN was motivated by visible light to produce electrons and holes. The photo-generated electrons migrate from the conduction band of g-C_3N_4 to the surface of SiO_2, resulting in inhibition of photo-generated charges recombination. Photo-induced electrons are captured by the oxygen adsorbed on the surface of the catalyst to generate $^{\bullet}O_2$. Because the conduction band potential of g-C_3N_4 (–1.05 eV) is much more negative than the reduction

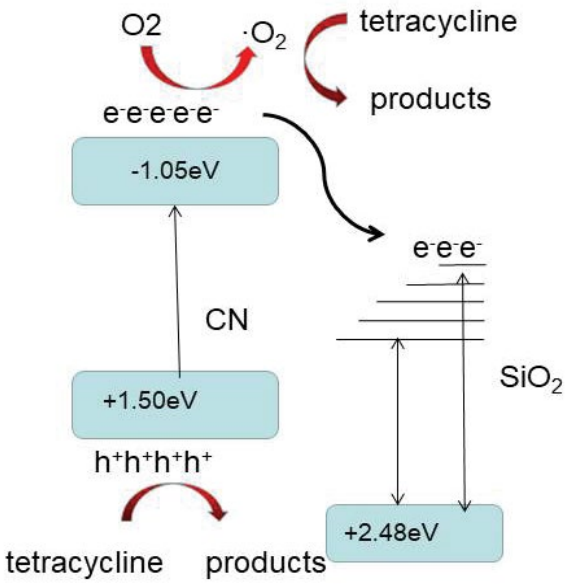

Fig. 10. Schematic illustration for photocatalytic degradation of tetracycline with SiO_2/CN-30.

potential of $O_2/^{\bullet}O_2^-$ (–0.33 eV), the produced $^{\bullet}O_2$ is main active species for degradation of tetracycline. In addition, $^{\bullet}O_2$ is reduced by electrons to form $^{\bullet}OH$, and $^{\bullet}OH$ participate in degradation of RhB to some extent. Due to the significantly positive valence band potential of g-C_3N_4, the photo-produced holes play a role in oxidizing tetracycline.

4. Conclusion

The g-C_3N_4/SiO_2 nanocomposite with significantly enlarged surface areas successfully synthesized using a facile vapor deposition. It is found that as-prepared g-C_3N_4/SiO_2 composite exists as core-shell formation in which incompact g-C_3N_4 is coated on the surface of SiO_2 nanoparticle. Compared to bluk g-C_3N_4, the specific surface areas of g-C_3N_4/SiO_2 composite enlarges evidently at a value of 97.32 m^2/g, which is 6.74 times as high as that of bluk g-C_3N_4 (14.44 m^2/g). The g-C_3N_4/SiO_2 composite exhibits significantly enhanced photocatalytic activity for degradation of tetracycline. Under the irradiation of visible-light, 72.7% of tetracycline can be degraded within 60 min. The photodegradation rate constant of tetracycline over g-C_3N_4/SiO_2 is 7.2 times as high as that over bulk g-C_3N_4. The greatly enhanced photocatalytic activity of g-C_3N_4/SiO_2 is attributed to not only enlarged specific surface areas but also the inhibition of photo-induced electron-hole pair recombination due to the existence of SiO_2. The active species in the degradation of tetracycline catalyzed by g-C_3N_4/SiO_2 are mainly superoxide radicals, followed by holes and hydroxyl radicals.

Acknowledgments

This work is supported by Postgraduate Research and Practice Innovation Program of Jiangsu Province, China (Grant Number: SJKY19_2629; SJKY19_2658).

References

[1] F.P. Cai, Y.B. Tang, F.Y. Chen, Y. Yan, W.D. Shi, Enhanced visible-light-driven photocatalytic degradation of tetracycline by Cr^{3+} doping $SrTiO_3$ cubic nanoparticles, RSC Adv., 5 (2015) 21290–21296.

[2] W. Liu, G. Zhao, M. An, L. Chang, Solvothermal synthesis of nanostructured $BiVO_4$ with highly exposed (010) facets and enhanced sunlight-driven photocatalytic properties, Appl. Surf. Sci., 357 (2015) 1053–1063.

[3] M.Y. Li, Y.B. Tang, W.L. Shi, F.Y. Chen, Y. Shi, H.C. Gu, Design of visible-light - response core-shell $Fe_2O_3/CuBi_2O_4$ heterojunctions with enhanced photocatalytic activity towards the degradation of tetracycline: Z-scheme photocatalytic mechanism insight, Inorg. Chem. Front., 5 (2018) 3148–3154.

[4] J. He, L. Chen, Z.Q. Yi, D. Ding, C.T. Au, S.F. Yin, Fabrication of two-dimensional porous CdS nanoplates decorated with C_3N_4 nanosheets for highly efficient photocatalytic hydrogen production from water splitting, Catal. Commun., 99 (2017) 79–82.

[5] J. Xu, B.Y. Luo, W. Gu, Y.P. Jian, F.L. Wu, Y.B. Tang, H. Shen. Fabrication of $In_2S_3/NaTaO_3$ composite for enhancing the photocatalytic activity toward the degradation of tetracycline, New J. Chem., 42 (2018) 5052–5058.

[6] Y.B. Tang, H.J. Yang, F.Y. Chen, X.G. Wang, Preparation, characterization of nanocomposites plasmonic photocatalyst C@(Fe_3O_4–halloysite nanotubes)-Ag/AgCl and its photocatalytic activity, Desal. Water Treat., 110 (2018) 144–153.

[7] F.Y. Chen, Y.M. Liu, X. Zhang, L.N. He, Y.B. Tang, Inorganic-framework molecularly imprinted CdS/TiO_2 for selectively photocatalytic degradation of di (2-ethylhexyl) phthalate, J. Chem. Soc. Pak., 41 (2019) 308–318.

[8] S. Dadashi-Silab, M.A. Tasdelen, B. Kiskan, Photochemically mediated atom transfer radical polymerization using polymeric semiconductor mesoporous graphitic carbon nitride, Macromol. Chem. Phys., 215 (2014) 675–681.

[9] L. Ge, F. Zuo, J. Liu, Q. Ma, C. Wang, D. Sun, Synthesis and efficient visible light photocatalytic hydrogen evolution of polymeric g-C_3N_4 coupled with CdS quantum dots, J. Phys. Chem. C, 116 (2012) 13708–13714.

[10] G. Li, Z. Lian, W. Wang, D. Zhang, H. Li, Nanotube-confinement induced sizecontrollable g-C_3N_4 quantum dots modified single-crystalline TiO_2 nanotube arrays for stable synergetic photoelectrocatalysis, Nano Energy, 19 (2016) 446–454.

[11] Y.X. Wang, H. Wang, F.Y. Chen, F. Cao, X.H. Zhao, S.G. Meng, Y.J. Cui, Facile synthesis of oxygen doped carbon nitride hollow microsphere for photocatalysis, Appl. Catal., B, 206 (2017) 417–425.

[12] S.W. Hu, L.W. Yang, Y. Tian, X.L. Wei, J.W. Ding, J.X. Zhong, P.K. Chu, Simultaneous nanostructure and heterojunction engineering of graphitic carbon nitride via *in situ* Ag doping for enhanced photoelectrochemical activity, Appl. Catal., B, 163 (2015) 611–622.

[13] J. Zhao, L. Ma, H. Wang, Y. Zhao, J. Zhang, S. Hu, Novel band gap-tunable K-Na co-doped graphitic carbon nitride prepared by molten salt method, Appl. Surf. Sci., 332 (2015) 625–630.

[14] K.C. Christoforidis, T. Montini, E. Bontempi, S. Zafeiratos, J.J. Delgado-Jaen, P. Fornasiero, Synthesis and photocatalytic application of visible-light active beta-Fe_2O_3/g-C_3N_4 hybrid nanocomposites, Appl. Catal., B, 187 (2016) 171–180.

[15] Q. Li, X. Li, S. Wageh, A.A. Al-Ghamdi, J.G. Yu, CdS/graphene nanocomposite photocatalysts, Adv. Energy Mater., 5 (2015) 28–30.

[16] I. Papailias, N. Todorova, T. Giannakopoulou, J. Yu, D. Dimotikali, C. Trapalis, Photocatalytic activity of modified g-C_3N_4/TiO_2 nanocomposites for NO*x* removal, Catal. Today, 280 (2017) 37–44.

[17] H. Hou, F. Gao, L. Wang, M. Shang, Z. Yang, J. Zheng, W. Yang, Superior thoroughly mesoporous ternary hybrid photocatalysts of TiO_2/WO_3/g-C_3N_4 nanofibers for visible-light-driven hydrogen evolution, J. Mater. Chem. A, 4 (2016) 6276–6281.

[18] B.Y. Peng, S.S. Zhang, S.Y. Yang, H.J. Wang, H. Yu, S.Q. Zhang, F. Peng, Synthesis and characterization of g-C_3N_4/Cu_2O composite catalyst with enhanced photocatalytic activity under visible light irradiation, Mater. Res. Bull., 56 (2014) 19–24.

[19] Z.Y. Zhang, J.D. Huang, M.Y. Zhang, Q. Yuan, B. Dong, Ultrathin hexagonal SnS_2 nanosheets coupled with g-C_3N_4 nanosheets as 2D/2D heterojunction photocatalysts toward high photocatalytic activity, Appl. Catal., B, 163 (2015) 298–305.

[20] C. Liu, D. Yang; Y. Jiao, Y. Tian, Y.G. Wang, Z.Y. Jiang, Biomimetic synthesis of TiO_2–SiO_2–Ag nanocomposites with enhanced visible-light photocatalytic activity, ACS Appl. Mater. Interfaces, 5 (2013) 3824–3832.

[21] Y. Tian, W. Li, C. Zhao, Y. Wang, B. Zhang, Q. Zhang, Fabrication of hollow mesoporous SiO_2-BiOCl@PANI@Pd photocatalysts to improve the photocatalytic performance under visible light, Appl. Catal., B, 213 (2017) 136–146.

[22] X. Zhang, F.Y. Chen, Y.B. Tang, Y.M. Liu, X.G. Wang, A rapid microwave synthesis of nanoscale $BiVO_4/Bi_2O_3$@SiO_2 with large specific surface area and excellent visible-light-driven activity, Desal. Water Treat., 152 (2019) 99–107.

[23] Y. Xu, W.D. Zhang, Sulfur/g-C_3N_4 composites with enhanced visible light photocatalytic activity, Sci. Adv. Mater., 6 (2014) 2611–2617.

[24] Z.J. Tong, D. Yang, Z. Li, F. Ding, Y. Shen, Z. Jiang, Thylakoid-inspired multishell g-C_3N_4, nanocapsules with enhanced visible-light harvesting and electron transfer properties for high-efficiency photocatalysis, ACS Nano, 11 (2017) 1103–1112.

[25] S. Zhang, M. Li, W. Qiu, Y. Wei, G. Zhang, J. Han, H. Wang, X. Liu, Super small polymeric carbon nitride nanospheres with core-shell structure for photocatalysis, ChemistrySelect, 2 (2017) 10580–10585.

[26] Q. Hao, X. Niu, C. Nie, S. Hao, W. Zou, J. Ge, D. Chen, W. Yao, A highly efficient g-C_3N_4/SiO_2 heterojunction: the role of SiO_2 in the enhancement of visible light photocatalytic activity, Phys. Chem. Chem. Phys., 18 (2016) 31410–31418.

[27] B. Lin, C. Xue, X. Yan, G. D. Yang, G. Yang, B. Yang, Facile fabrication of novel SiO_2/g-C_3N_4 core-shell nanosphere photocatalysts with enhanced visible light activity, Appl. Surf. Sci., 357 (2015) 346–355.

[28] X. Wang, S. Wang, W. Hu, J. Cai, L. Zhang, L. Dong, L. Zhao, Y. He, Synthesis and photocatalytic activity of SiO_2/g-C_3N_4 composite photocatalyst, Mater. Lett., 115 (2014) 53–56.

[29] Y. Tan, Z. Shu, J. Zhou, T. Li, W. Wang, Z. Zhao, One-step synthesis of nanostructured g-C_3N_4/TiO_2 composite for highly enhanced visible-light photocatalytic H_2 evolution. Appl. Catal., B, 230 (2018) 260–268.

[30] Q. Xiang, J. Yu, M. Jaroniec, Preparation and enhanced visible-light photocatalytic H_2-production activity of graphene/C_3N_4 composites, J. Phys. Chem. C, 115 (2011) 7355–7363.